First Experimental Limit on the Permanent Electric Dipole Moment of the Deuteron

A. Andres,[1,2,*] V. Hejny,[2] A. Nass,[2] N. N. Nikolaev,[3,†] J. Pretz,[1,2] F. Rathmann,[2,‡] V. Shmakova,[4,‡] J. Slim,[1,§] F. Abusaif,[1,2,‖] A. Aggarwal,[5] A. Aksentev,[6] B. Alberdi,[1,2,¶] L. Barion,[4] I. Bekman,[2,**] M. Beyß,[1,2] C. Böhme,[2] B. Breitkreutz,[2] N. Canale,[4] G. Ciullo,[4] S. Dymov,[4] N.-O. Fröhlich,[2,‖] R. Gebel,[2] M. Gaisser,[1] K. Grigoryev,[2,*] D. Grzonka,[2] D. Gu,[1,7] D. Heberling,[8] J. Hetzel,[2,*] D. Hölscher,[8] O. Javakhishvili,[9,††] A. Kacharava,[2] V. Kamerdzhiev,[2,*] S. Karanth,[5,‡‡] I. Keshelashvili,[2,*] A. Kononov,[4] K. Laihem,[1,*] A. Lehrach,[1,2] P. Lenisa,[4] N. Lomidze,[10] B. Lorentz,[7] G. Macharashvili,[10] A. Magiera,[5] M. Margos,[1,7] D. Mchedlishvili,[10] A. Melnikov,[6] F. Müller,[1,2] D. Okropiridze,[10,§§] A. Pesce,[2] A. Piccoli,[4] V. Poncza,[2] D. Prasuhn,[2] A. Saleev,[4,‖‖] D. Shergelashvili,[10] R. Shankar,[4] N. Shurkhno,[2,*] S. Siddique,[1,2,*] A. Silenko,[11] H. Soltner,[12] R. Stassen,[2] E. J. Stephenson,[13] H. Ströher,[2] M. Tabidze,[10] G. Tagliente,[14] V. Tempel,[1,7] Y. Valdau,[2,*] M. Vitz,[1,2] T. Wagner,[1,2,*] A. Wirzba,[15] A. Wrońska,[5] P. Wüstner,[12] and M. Żurek[2,¶¶]

(JEDI Collaboration)

[1]*III. Physikalisches Institut B, RWTH Aachen University, 52056 Aachen, Germany*
[2]*Institut für Kernphysik, Forschungszentrum Jülich, 52425 Jülich, Germany*
[3]*L.D. Landau Institute for Theoretical Physics, 142432 Chernogolovka, Russia*
[4]*University of Ferrara and Istituto Nazionale di Fisica Nucleare, 44100 Ferrara, Italy*
[5]*Marian Smoluchowski Institute of Physics, Jagiellonian University, 30348 Cracow, Poland*
[6]*Institute for Nuclear Research, Russian Academy of Sciences, 117312 Moscow, Russia*
[7]*GSI Helmholtzzentrum für Schwerionenforschung GmbH, Planckstraße 1, 64291 Darmstadt, Germany*
[8]*Institut für Hochfrequenztechnik, RWTH Aachen University, 52056 Aachen, Germany*
[9]*Department of Electrical and Computer Engineering, Agricultural University of Georgia, 0159 Tbilisi, Georgia*
[10]*High Energy Physics Institute, Tbilisi State University, 0186 Tbilisi, Georgia*
[11]*Bogoliubov Laboratory of Theoretical Physics, International Intergovernmental Organization Joint Institute for Nuclear Research, 141980 Dubna, Russia*
[12]*Institute of Technology and Engineering, Forschungszentrum Jülich, 52425 Jülich, Germany*
[13]*Indiana University, Department of Physics, Bloomington, Indiana 47405, USA*
[14]*Istituto Nazionale di Fisica Nucleare sez. Bari, 70125 Bari, Italy*
[15]*Institute for Advanced Simulation, Forschungszentrum Jülich, 52425 Jülich, Germany*

(Received 24 February 2026; accepted 27 April 2026; published 16 June 2026)

Permanent electric dipole moments (EDMs) provide a sensitive probe of physics beyond the standard model and are directly linked to additional sources of *CP* violation that could explain the matter-antimatter asymmetry of the Universe. EDM measurements of charged particles in storage rings rely on detecting a small tilt of the invariant spin axis with respect to the ring plane. In this Letter, we present the experimental

[*]Present address: GSI Helmholtzzentrum für Schwerionenforschung GmbH, Planckstr. 1, 64291 Darmstadt, Germany.
[†]Present address: N.N. Bogoliubov Laboratory of Theoretical Physics, 141980 Dubna, Russia.
[‡]Present address: Brookhaven National Laboratory, Upton, New York 11973, USA.
[§]Present address: Deutsches Elektronen-Synchrotron, 22607 Hamburg, Germany.
[‖]Present address: Karlsruhe Institute of Technology, Hermannvon-Helmholtz-Platz 1, 76344 Eggenstein-Leopoldshafen, Germany.
[¶]Present address: Humboldt-Universität zu Berlin, Institut für Physik, Newton-Straße 15, 12489 Berlin, Germany.
[**]Present address: Institute of Technology and Engineering, Forschungszentrum Jülich, 52425 Jülich, Germany.
[††]Present address: Faculty of Nuclear Sciences and Physical Engineering, Czech Technical University in Prague, 160 00 Praha 6, Czech Republic.
[‡‡]Present address: H. Niewodniczański Institute of Nuclear Physics, Polish Academy of Sciences, 31342, Kraków, Poland.
[§§]Present address: Ruhr-Universität Bochum, Institut für Experimentalphysik I, 44801 Bochum, Germany.
[‖‖]Present address: Institut für nachhaltige Wasserstoffwirtschaft, Forschungszentrum Jülich, 52425 Jülich, Germany.
[¶¶]Present address: Argonne National Laboratory, Lemont, Illinois 60439, USA.

determination of the invariant spin axis of an ensemble of deuterons in the Cooler Synchrotron (COSY), a conventional magnetic storage ring, using a combination of a radio-frequency Wien filter, a superconducting Siberian snake, and an electron-cooler solenoid. The measurements reveal tilts of a few milliradians, which are dominated by systematic effects. From the observed tilts, we derive the first experimental limit on the deuteron EDM, $|d^d| < 2.5 \times 10^{-17}\ e\,\mathrm{cm}$(95% C.L.). This result demonstrates the feasibility of using storage rings to search for EDMs of charged stable hadrons and provides a foundation for future dedicated facilities.

DOI: 10.1103/ns3s-ld4k

Permanent electric dipole moments (EDMs) of elementary and composed subatomic particles violate both parity (P) and time-reversal (T) symmetry [1,2]. If the combined CPT symmetry, where C represents charge conjugation, is conserved, then T violation implies CP violation [3,4]. So far CP violation have been observed, for example, in the decays of neutral kaons [5], B mesons [6,7], and baryons [8]. The standard model predicts EDMs so tiny that their detection is beyond the current experimental reach [9,10]. Consequently, any measurable EDM would be a hint at the presence of physics beyond the standard model (or a nonzero QCD θ term) [2]. Therefore, EDMs are considered to be sensitive probes to search for additional sources of CP violation, which are needed to explain the observed matter-antimatter asymmetry in the Universe [11]. This Letter discusses the first measurement of the deuteron EDM building on a sequence of milestones previously achieved and published by the JEDI Collaboration [12–16].

In general, an EDM of a subatomic particle can be measured by studying its influence on the particle's spin motion, since the EDM is aligned with its spin direction. Quantitatively, the spin dynamics is governed by the Thomas–Bargmann-Michel-Telegdi equation [17–19]. In a purely magnetic storage ring with a vertical magnetic field and $\vec{\beta} \perp \vec{B}$, the spin evolution relative to the momentum vector can be described in a corotating frame. Subtracting the cyclotron rotation removes all kinematic and Dirac ($g = 2$) contributions, such that the remaining spin precession is governed solely by the anomalous magnetic moment G and a possible EDM (see, e.g., Ref. [10]). Neglecting terms proportional to $\vec{\beta} \cdot \vec{B}$, the resulting equation of motion reads

$$\frac{\mathrm{d}\vec{S}}{\mathrm{d}t} = \vec{\Omega}_S \times \vec{S} = (\vec{\Omega}_G + \vec{\Omega}_{\mathrm{EDM}}) \times \vec{S}, \tag{1}$$

$$\vec{\Omega}_G = -\frac{q}{m} G \vec{B}, \tag{2}$$

$$\vec{\Omega}_{\mathrm{EDM}} = -\frac{q}{m}\frac{\eta}{2}\vec{\beta} \times \vec{B}. \tag{3}$$

Here, $\vec{\Omega}_G$ denotes exclusively the anomalous magnetic-moment-induced spin precession and $\vec{\Omega}_{\mathrm{EDM}}$ the EDM-induced spin rotation. $\vec{S}$ is the spin vector in units of $\hbar$ in the particle rest frame, t the time in the laboratory system, m and q the rest mass and the charge of the particle, β the particle velocity in units of c, and $\vec{B}$ the magnetic field in the laboratory system. The dimensionless quantities G and η are related to the magnetic dipole moment $\vec{\mu}$ and the EDM $\vec{d}$,

$$\vec{\mu} = g\frac{q\hbar}{2m}\vec{S} = (1+G)\frac{q\hbar}{m}\vec{S} \quad \text{and} \quad \vec{d} = \eta\frac{q\hbar}{2mc}\vec{S}. \tag{4}$$

With the given assumptions, the anomalous magnetic moment and an EDM cause precessions around the vertical y axis and the radial x axis, respectively (see Fig. 1),

$$\vec{\Omega}_G = \Omega_G \vec{e}_{\mathrm{y}}, \tag{5}$$

$$\vec{\Omega}_{\mathrm{EDM}} = \Omega_{\mathrm{EDM}} \vec{e}_{\mathrm{x}}. \tag{6}$$

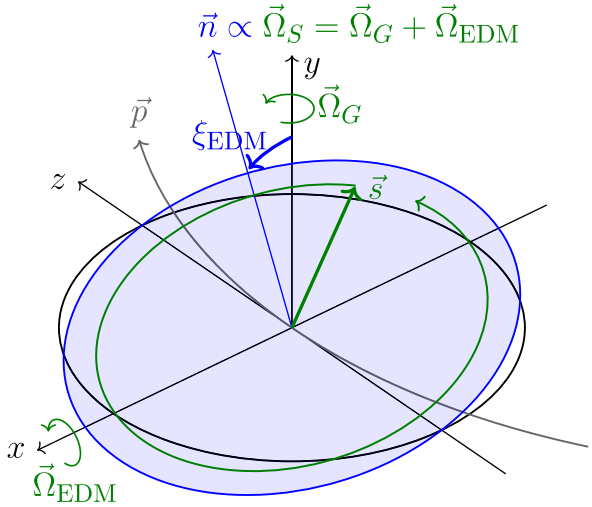

FIG. 1. Influence of the EDM on the invariant spin axis $\vec{n}$. The gray line marks the beam trajectory. Assuming an idealized storage ring and no EDM, the spin is precessing in the x-z plane. A non-zero EDM tilts the spin-precession plane around the z-axis by an angle ξ_{EDM} indicated by the blue plane. The situation shown here corresponds to a particle with $G < 0$, e.g. a deuteron. The spin $\vec{s}$ precesses in opposite direction to the momentum $\vec{p}$. For a positive EDM, i.e. $\eta > 0$, the angle ξ_{EDM} defined in Eq. (8) is negative.

It is convenient to introduce the invariant spin axis $\vec{n}$ as a unit vector normal to the tilted precession plane, i.e., $\vec{\Omega}_S = \Omega_S \vec{n}$, and its tilt angle ξ_{EDM} in the x-y plane such that

$$\vec{n} = (-\sin\xi_{\mathrm{EDM}}, \cos\xi_{\mathrm{EDM}}, 0). \tag{7}$$

With $|\eta| \ll 1$ one gets to first order in η

$$\xi_{\mathrm{EDM}} = -\frac{\Omega_{\mathrm{EDM}}}{\Omega_G} = \frac{\eta\beta}{2G}. \tag{8}$$

Solving Eq. (1) one finds for a spin vector initially pointing in the longitudinal direction $[\vec{S}(0) = (0,0,1)]$ to first order in η,

$$\vec{S}(t) = \left(\sin(\Omega_G t), \xi_{\mathrm{EDM}} \sin(\Omega_G t), \cos(\Omega_G t)\right), \tag{9}$$

i.e., the EDM causes an oscillation of the vertical polarization component with amplitude $|\xi_{\mathrm{EDM}}|$. This signature is used in the muon $g-2$ experiment to measure the muon EDM [20]. For deuterons this approach is far less sensitive because the magnitude of the magnetic anomaly G is much larger than that of the muon.

To induce a macroscopic buildup of a vertical polarization an additional radio-frequency (rf) Wien filter [21,22] in resonance with the spin precession is applied such that the Lorentz force vanishes [23] and the electric and magnetic fields only act on the spin vector. For a bunched beam, the rf Wien filter applies a spin kick turn by turn and is operated at a spin-resonance frequency corresponding to the k th harmonic of the revolution frequency. The additional spin rotation around the magnetic field axis $\vec{m}$ of the rf Wien filter (WF) per turn is

$$\psi(t) = \psi_0 \sin(\Omega_{\mathrm{WF}} t + \varphi_{\mathrm{rel}}) \quad \text{with} \tag{10}$$

$$\psi_0 = \frac{q}{m}\frac{G+1}{\gamma^2\beta c}\int B_{\mathrm{WF}}\mathrm{d}l, \tag{11}$$

$$\Omega_{\mathrm{WF}} = |k\Omega_{\mathrm{rev}} + \Omega_S|, \quad k \in \mathbb{Z}, \tag{12}$$

where B_{WF} and Ω_{WF} denote the magnetic field and the radio frequency of the rf Wien filter, respectively, and φ_{rel} is the relative phase between the radio frequency and the precession in the horizontal plane. The corresponding spin dynamics is presented in detail in Refs. [24,25]. Below, only the key elements are summarized.

Solving Eq. (1) for this case, the fast vertical oscillation in Eq. (9) is superimposed by a slow oscillation (also see Fig. 10 of Ref. [16]),

$$S_y(t) = \cos(\varphi_{\mathrm{rel}}) \sin(2\pi f_y t). \tag{13}$$

The frequency f_y depends on the relative orientation of the magnetic-field axis $\vec{m}$ and the static invariant spin axis $\vec{n}$ in the absence of the rf excitation. Aligned axes do not induce an oscillation, whereas a perpendicular configuration yields the maximal effect. If $\vec{m}$ is vertical, this sensitivity allows the rf Wien filter to probe the tilt of the invariant spin axis. As experimental observable one can then define the resonance tune (or resonance strength) directly related to ξ_{EDM},

$$\epsilon = \frac{f_y}{f_{\mathrm{rev}}} = \frac{\psi_0}{4\pi}|\vec{n}\times\vec{m}| = \frac{\psi_0}{4\pi}|\sin(\xi_{\mathrm{EDM}})|. \tag{14}$$

This describes the ideal case where only the EDM contributes to the tilt of $\vec{n}$. In an actual ring, however, magnet misalignments, field imperfections, and orbit deviations introduce additional, position-dependent contributions n_x^{sys} and n_z^{sys},

$$\vec{n} = \left(n_x^{\mathrm{sys}} - \xi_{\mathrm{EDM}}, 1, n_z^{\mathrm{sys}}\right) \text{ for } |\xi_{\mathrm{EDM}}|, |n_x^{\mathrm{sys}}|, |n_z^{\mathrm{sys}}| \ll 1. \tag{15}$$

Therefore, instead of aligning the rf Wien filter's magnetic field axis $\vec{m}$ vertically and measuring only the buildup, we followed a different strategy. The rf Wien filter could be rotated around the beam axis (ϕ_{WF}) to introduce an additional x component (roll) to $\vec{m}$, while a spin rotation in a Siberian snake located on the opposite side of the ring (see Fig. 2) added a z component (pitch) to $\vec{n}$ (ϕ_{snake}). For small additional tilts one gets

$$\vec{n} = (n_x, 1, n_z + \phi_{\mathrm{snake}}), \tag{16}$$

$$\vec{m} = (\phi_{\mathrm{WF}}, 1, 0), \tag{17}$$

and using Eq. (14) ϵ^2 can be written in leading order as

$$\epsilon^2 = \frac{\psi_0^2}{16\pi^2}\left[(n_x - \phi_{\mathrm{WF}})^2 + (n_z + \phi_{\mathrm{snake}})^2\right]. \tag{18}$$

Equation (18) describes a two-dimensional paraboloid with the minimum corresponding to $\vec{m}\|\vec{n}$, where the resonance strength vanishes. The corresponding angles $\phi_{\mathrm{WF}}^{\mathrm{min}}$

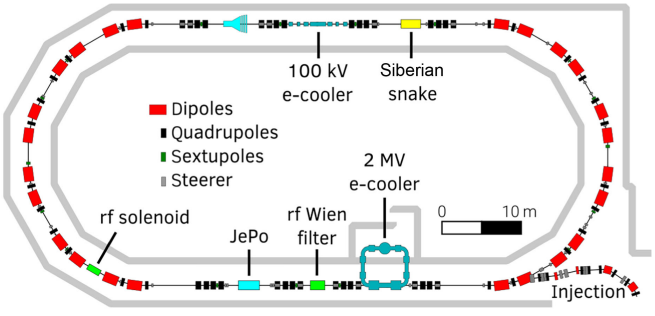

FIG. 2. Sketch of the COSY ring indicating the position of the relevant installations: electron coolers, rf Wien filter, Siberian snake and the JEDI polarimeter (JePo).

TABLE I. Beam and machine parameters. The deuteron mass m and the deuteron g factor are taken from the National Institute of Standards and Technology database [30].

Parameter	Symbol	Unit	Value
Deuteron momentum (lab)	p	[MeV/c]	970
Particles per bunch	N		$(0.5-1)\times 10^9$
Lorentz factor	γ		1.126
Beam velocity	β		0.46
COSY circumference	L_{COSY}	[m]	183.6
Revolution frequency	f_{rev}	[Hz]	750602.6
Spin precession frequency	f_s	[Hz]	120847.3
Deuteron mass	m	[MeV/c^2]	1875.61
Deuteron g factor	g		1.714025
Deuteron $G=(g-2)/2$	G		−0.142987
rf Wien filter field integral	$\int B_{\mathrm{WF}}\mathrm{d}l$	[μTm]	7.9 − 12.0

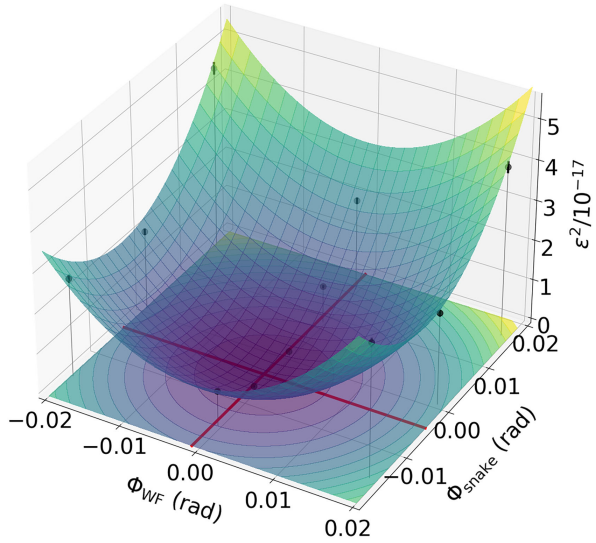

FIG. 3. The resonance strength for Map 2 bunch 1 is shown as a function of the rf Wien filter rotation angle and the spin rotation in the Siberian snake. The minimum of the resulting two-dimensional paraboloid indicates the orientation of the invariant spin axis at the location of the rf Wien filter.

and $\phi^{\mathrm{min}}_{\mathrm{snake}}$ are a measure of the direction of the invariant spin axis at the rf Wien filter location such that $\vec{n}=(\phi^{\mathrm{min}}_{\mathrm{WF}},1,-\phi^{\mathrm{min}}_{\mathrm{snake}})$. This approach facilitates a systematic study of how experimental uncertainties affect the extracted parameters and the final result.

The experiment was performed at the Cooler Synchrotron (COSY) at Forschungszentrum Jülich, utilizing the standard COSY infrastructure along with the rf Wien filter [23], a superconducting Siberian snake [26,27], the solenoid of the 2-MV electron cooler (e-cooler), and the JEDI polarimeter (JePo) [28] (see Fig. 2). Results from beam-based alignment [29] and a dedicated geodetic survey of the ring magnets were implemented following the experience gained in earlier experiments. A summary of standard parameters is given in Table I. Each cycle involved the injection of vertically (vector)polarized deuterons into the COSY ring, bunching and accelerating the beam to 970 MeV/c, electron cooling to reduce emittance and orbit corrections. After starting the extraction onto a carbon target for polarization measurements the deuteron spins were rotated into the horizontal plane using an rf solenoid. The spin precession was continuously monitored, and the rf frequency and phase of the Wien filter was adjusted accordingly to keep a constant phase between the Wien filter rf and the spin precession phase (phase locking) [13,16].

The experiment began with spin-coherence time optimization [12,31], followed by systematic studies of the vertical polarization buildup. The data acquisition system was the same as described in [16]. The primary observables were the detector rates in the four quadrants up, right, down, left of JePo together with the radio frequencies of the accelerator cavity and the rf Wien filter. The rates were used to calculate the time-dependent up-down and left-right asymmetry as a measure of the in-plane and vertical polarization, respectively.

The measurements were organized in maps, defined as two-dimensional scans over ϕ_{WF} and ϕ_{snake}, each at various relative phases φ_{rel}, with all other parameters held fixed for one map. For this, the two methods discussed conceptually in [16] were used: (i) one or more bunches, such that the phase locking is probing the same bunch as reference that the rf Wien filter acts on (single-bunch method), and (ii) using two bunches with the rf Wien filter selectively acting on one bunch while the other bunch remained undisturbed (pilot-bunch method) [15].

In order to determine the resonance strength ϵ, the in-plane and vertical polarizations were fitted simultaneously using model-based fit functions [25,32], with common parameters describing the resonance strength, oscillation amplitude, spin decoherence, and the deviation from resonance. The corresponding fit formulas are given in End Matter. The squared resonance strength (ϵ^2) is then plotted as a function of ϕ_{WF} and ϕ_{snake}, as exemplarily shown in Fig. 3. The minimum, and thus the direction of the invariant spin axis, is extracted by a parabolic fit using Eq. (18).

In total, seven maps were taken: the first two using the single-bunch method and the remaining five using the pilot-bunch method. The measurement of each map took approximately 24 h. For systematic studies, the last two maps were taken with the 2-MV e-cooler solenoid inducing an additional tilt of an invariant spin axis at the location of the rf Wien filter of $\Delta n_x=\pm 1$ mrad and $\Delta n_z=\pm 1.8$ mrad; the plus signs apply to map 6 and the minus signs to map 7. The results are summarized in Table II; the quoted uncertainties are statistical only. The elevated reduced chi-squared values and the observed scatter reflect varying systematic offsets throughout the data, which dominate the chi-squared contributions at larger distances from the minimum. Averaging yields

TABLE II. Summary of all maps of the invariant spin axis. Maps 6 and 7 were taken with the 2-MV e-cooler solenoid inducing an additional, fixed tilt of the invariant spin axis at the location of the rf Wien filter. The corresponding shift of the minimum has been taken into account.

Map	n_x/mrad	n_z/mrad	χ^2/ndf	Method
1	−1.72(12)	4.90(6)	455.5/8 = 56.9	Single bunch
2	−1.34(11)	4.18(4)	147.0/8 = 18.4	Single bunch
3	−3.29(36)	3.54(31)	16.5/5 = 3.3	Pilot bunch
4	−1.96(8)	3.81(4)	163.8/21 = 7.8	Pilot bunch
5	−2.50(8)	3.61(5)	201.8/21 = 9.6	Pilot bunch
6	−0.61(12)	3.15(6)	52.5/5 = 10.5	Pilot bunch
7	−4.84(17)	3.35(10)	127.5/5 = 25.5	Pilot bunch

$$n_{x,\text{avg.}} = -2.1(12)\,\text{mrad}, \quad n_{z,\text{avg.}} = 3.9(6)\,\text{mrad}, \quad (19)$$

where the uncertainties correspond to the rms of the scatter of the results. These results are clearly dominated by systematic effects. Ideally, n_x would be a measure of the EDM effect, while n_z would be consistent with zero.

The experimental method relies on the magnetic-field axis of the rf Wien filter as a reference for determining the orientation of the invariant spin axis. While no direct experimental data exist on the magnetic-field direction within the rf Wien filter, extensive simulation studies have been performed, which explore the range of possible field errors perpendicular to the main axis [23,33,34]. Additional simulations were performed that explicitly account for the geometry of the installed rf Wien filter, following the approach described in Ref. [33]. The resulting possible spread corresponds to systematic uncertainties in the order of a few milliradians in the field orientation. The dominant contribution was found to originate from a rotation of the beam axis in the horizontal plane. Further details are given in End Matter.

Extensive beam and spin-tracking simulations to study the influence of known misalignments of the ring magnets and the beam-position monitors and the corresponding uncertainties have been carried out. No longitudinal or radial components of the invariant spin axis larger than 1 mrad could be found [35].

As a further systematic check, the longitudinal component of the invariant spin axis at the locations of two solenoids was determined using the spin tune mapping [14] developed by the JEDI Collaboration. In these measurements the rf Wien filter was not involved. The results are

$$n_{z,1} = -0.0565(7)\,\text{mrad}, \quad n_{z,2} = -0.0706(6)\,\text{mrad}, \quad (20)$$

for the Siberian snake and the 2-MV e-cooler solenoid, respectively. The longitudinal tilt below 0.1 mrad, measured at the 2-MV e-cooler solenoid only 8m upstream of the rf Wien filter, supports the conclusion that the main systematic uncertainties originate from the direction of the magnetic field axis of the rf Wien filter.

In an ideal storage ring, the invariant spin axis has no longitudinal component. As the observed longitudinal tilt is therefore predominantly caused by systematic effects, the measured tilt provides a direct estimate of the experimental uncertainty. This uncertainty can then be transferred to the radial component in order to construct an upper limit for the corresponding tilt,

$$\sigma_{n_z^{\text{sys}}} \approx \sigma_{n_x^{\text{sys}}} \hat{=} n_{z,\text{avg.}} = 3.9\ \text{mrad}. \quad (21)$$

Assuming that our measurement is consistent with an EDM value of zero and taking $\sigma_{n_z^{\text{sys}}} = 3.9$ mrad as a one standard deviation Gaussian error for n_x, a 95% C.L. can be obtained by multiplying by the corresponding factor 1.96. Using Eqs. (7) and (8), this translates into an upper limit of the dimensionless EDM strength,

$$|\eta| < 0.00475\ (95\%\ \text{C.L.}). \quad (22)$$

Consequently, a first limit on the deuteron EDM can be determined using Eq. (4),

$$|d^d| < 2.5 \times 10^{-17}\ e\,\text{cm}\,(95\%\,\text{C.L.}). \quad (23)$$

To put this result into perspective, the only measurement of a permanent EDM performed in a storage ring so far was carried out for muons, yielding an upper limit of $|d^\mu| < 1.8 \times 10^{-19}\ e\,\text{cm}\,(95\%\,\text{C.L.})$ [20]. The sensitivity is governed by the ratio of the EDM to the magnetic anomaly, $G \approx -0.14$ for deuterons and $a \simeq 0.001$ for muons, resulting in about 2 orders of magnitude higher sensitivity for the muon. Furthermore, this result was obtained using a dedicated muon storage ring specifically designed for precision experiments. It should also be noted that at COSY a significantly more stringent limit has recently been obtained for an axion-field-induced oscillating EDM of the deuteron [36]. Owing to the resonant coupling to the axion field, most systematic effects cancel, illustrating the potential of storage-ring techniques.

This measurement demonstrates that a storage ring can be used to access the EDM of charged hadrons by precisely determining the invariant spin axis. At the present stage, the observed tilt of the invariant spin axis is still dominated by systematic effects, such as magnet misalignments, deviations from an ideal orbit, and field errors. This calls for further experimental studies aimed at reducing and validating the associated systematic uncertainties. An improved rf Wien filter setup, incorporating additional ferrites to enhance field strength and homogeneity, had already been prepared for implementation. However, the COSY ring was permanently shut down at the end of 2023 and is no longer available for experiments.

Dedicated storage rings with only electric fields or a combination of electric and magnetic fields employing counterrotating beams are currently under investigation [37–39]. In such a configuration, many of the dominant systematic effects—arising from field imperfections, orbit distortions, and beam dynamics—are expected to cancel out due to their opposite signs in the two oppositely circulating beams. This cancellation offers a powerful pathway to significantly reduce systematic uncertainties and achieve a sensitivity that could surpass current limits for hadrons, i.e., 10^{-26} e cm for the neutron [40]. The successful realization of such a facility would mark a significant advance in precision EDM measurements, enabling a direct test of CP violation in the hadronic sector and opening a new frontier in the search for physics beyond the standard model.

Acknowledgments—We thank the COSY crew for their dedicated support in operating the accelerator during the experiment. This work was carried out within the framework of the JEDI Collaboration and supported by an ERC Advanced Grant from the European Union (Proposal No. 694340: *Search for Electric Dipole Moments Using Storage Rings*). The contributions of A. A., A. M., and N. N. N. were supported by the Russian Science Foundation (Grant No. 25-72-30005). This research also received funding from the European Union's Horizon 2020 research and innovation program under Grant Agreement STRONG-2020-No. 824093. The presented results are based on the Ph.D. thesis of A. A. [41].

Data availability—The data that support the findings of this article are openly available [42].

[1] I. B. Khriplovich and S. K. Lamoreaux, *CP Violation Without Strangeness: Electric Dipole Moments of Particles, Atoms, and Molecules* (Springer, New York, 1997).
[2] M. Pospelov and A. Ritz, Electric dipole moments as probes of new physics, Ann. Phys. (Amsterdam) **318**, 119 (2005).
[3] G. Lüders, Proof of the TCP theorem, Ann. Phys. (N.Y.) **2**, 1 (1957).
[4] O. W. Greenberg, CPT violation implies violation of Lorentz invariance, Phys. Rev. Lett. **89**, 231602 (2002).
[5] J. H. Christenson, J. W. Cronin, V. L. Fitch, and R. Turlay, Evidence for the 2π decay of the K_2^0 meson, Phys. Rev. Lett. **13**, 138 (1964).
[6] T. Gershon and V. V. Gligorov, CP violation in the B system, Rep. Prog. Phys. **80**, 046201 (2017).
[7] B. Aubert *et al.* (*BABAR* Collaboration), Observation of CP violation in the B^0 meson system, Phys. Rev. Lett. **87**, 091801 (2001).
[8] R. Aaij *et al.* (LHCb Collaboration), Observation of charge–parity symmetry breaking in baryon decays, Nature (London) **643**, 1223 (2025).
[9] J. Engel, M. J. Ramsey-Musolf, and U. van Kolck, Electric dipole moments of nucleons, nuclei, and atoms: The standard model and beyond, Prog. Part. Nucl. Phys. **71**, 21 (2013).
[10] T. E. Chupp, P. Fierlinger, M. J. Ramsey-Musolf, and J. T. Singh, Electric dipole moments of atoms, molecules, nuclei, and particles, Rev. Mod. Phys. **91**, 015001 (2019).
[11] A. D. Sakharov, Violation of CP invariance, C asymmetry, and baryon asymmetry of the universe, Sov. Phys. Usp. **34**, 392 (1991), reprint of: Pis'ma Zh. Eksp. Teor. Fiz. **5**, 32 (1967).
[12] G. Guidoboni *et al.* (JEDI Collaboration), How to reach a thousand-second in-plane polarization lifetime with 0.97-GeV/c deuterons in a storage ring, Phys. Rev. Lett. **117**, 054801 (2016).
[13] D. Eversmann *et al.* (JEDI Collaboration), New method for a continuous determination of the spin tune in storage rings and implications for precision experiments, Phys. Rev. Lett. **115**, 094801 (2015).
[14] A. Saleev *et al.* (JEDI Collaboration), Spin tune mapping as a novel tool to probe the spin dynamics in storage rings, Phys. Rev. Accel. Beams **20**, 072801 (2017).
[15] J. Slim *et al.* (JEDI Collaboration), Proof-of-principle demonstration of a pilot bunch comagnetometer in a stored beam, Phys. Rev. Res. **7**, 023257 (2025).
[16] V. Hejny *et al.* (JEDI Collaboration), Maintaining a resonance condition of an rf spin rotator through a feedback loop in a storage ring, Phys. Rev. Accel. Beams **28**, 062801 (2025).
[17] V. Bargmann, L. Michel, and V. L. Telegdi, Precession of the polarization of particles moving in a homogeneous electromagnetic field, Phys. Rev. Lett. **2**, 435 (1959).
[18] D. F. Nelson, A. A. Schupp, R. W. Pidd, and H. R. Crane, Search for an electric dipole moment of the electron, Phys. Rev. Lett. **2**, 492 (1959).
[19] T. Fukuyama and A. J. Silenko, Derivation of generalized Thomas-Bargmann-Michel-Telegdi equation for a particle with electric dipole moment, Int. J. Mod. Phys. A **28**, 1350147 (2013).
[20] G. W. Bennett *et al.* [Muon (g-2) Collaboration], Improved limit on the muon electric dipole moment, Phys. Rev. D **80**, 052008 (2009).
[21] F. Rathmann, A. Saleev, and N. N. Nikolaev (JEDI Collaboration and srEDM Collaboration), The search for electric dipole moments of light ions in storage rings, J. Phys. Conf. Ser. **447**, 012011 (2013).
[22] W. M. Morse, Y. F. Orlov, and Y. K. Semertzidis, rf Wien filter in an electric dipole moment storage ring: The "partially frozen spin" effect, Phys. Rev. ST Accel. Beams **16**, 114001 (2013).
[23] J. Slim *et al.*, Electromagnetic simulation and design of a novel waveguide rf Wien filter for electric dipole moment measurements of protons and deuterons, Nucl. Instrum. Methods Phys. Res., Sect. A **828**, 116 (2016).
[24] F. Rathmann, N. N. Nikolaev, and J. Slim, Spin dynamics investigations for the electric dipole moment experiment, Phys. Rev. Accel. Beams **23**, 024601 (2020).
[25] N. N. Nikolaev *et al.* (JEDI Collaboration), Spin decoherence and off-resonance behavior of radio-frequency-driven spin rotations in storage rings, Phys. Rev. Accel. Beams **27**, 111002 (2024).

[26] A. Lehrach and R. Maier, Siberian snake for the cooler synchrotron COSY, in *PACS2001. Proceedings of the 2001 Particle Accelerator Conference (Cat. No.01CH37268)*, Vol. 4 (IEEE, Chicago, IL, 2001), pp. 2566–2568, 10.1109/PAC.2001.987833.
[27] A. Lehrach, Commissioning of the Siberian snake in COSY (5th COSY Beam Time Advisory Committee, Bad Honnef (Germany), 19 Dec 2016–20 Dec 2016, 2016).
[28] F. Müller *et al.*, A new beam polarimeter at COSY to search for electric dipole moments of charged particles, J. Instrum. **15**, P12005 (2020).
[29] T. Wagner *et al.*, Beam-based alignment at the cooler synchrotron COSY as a prerequisite for an electric dipole moment measurement, J. Instrum. **16**, T02001 (2021).
[30] National Institute of Standards and Technology, Nist database, https://physics.nist.gov/cuu/Constants/index.html (2025), accessed: 2025-08-14.
[31] G. Guidoboni *et al.* (JEDI Collaboration), Connection between zero chromaticity and long in-plane polarization lifetime in a magnetic storage ring, Phys. Rev. Accel. Beams **21**, 024201 (2018).
[32] N. Hempelmann, Polarization measurement and manipulation for electric dipole moment measurements in storage rings, Dissertation, RWTH Aachen University, Aachen, 2018, 10.18154/RWTH-2018-221496.
[33] J. Slim, F. Rathmann, A. Nass, H. Soltner, R. Gebel, J. Pretz, and D. Heberling, Polynomial chaos expansion method as a tool to evaluate and quantify field homogeneities of a novel waveguide rf Wien filter, Nucl. Instrum. Methods Phys. Res., Sect. A **859**, 52 (2017).
[34] J. Slim, A novel waveguide rf Wien filter for electric dipole moment measurements of deuterons and protons at the COoler SYnchrotron (COSY)/Jülich, Dissertation, Rheinisch-Westfälische Technische Hochschule Aachen, Aachen, 2018, 10.18154/RWTH-2018-229484.
[35] M. Vitz, Investigation of systematic effects and uncertainties involved in the determination of the invariant spin axis in a storage ring for an EDM measurement,, Dissertation, RWTH Aachen University, Aachen, 2024, 10.18154/RWTH-2024-11202.
[36] S. Karanth *et al.* (JEDI Collaboration), First search for axionlike particles in a storage ring using a polarized deuteron beam, Phys. Rev. X **13**, 031004 (2023).
[37] F. Abusaif *et al.*, Storage ring to search for electric dipole moments of charged particles: feasibility study, Report No. CERN-2021-003, CERN, 2021, 10.23731/CYRM-2021-003.
[38] V. Anastassopoulos *et al.*, A storage ring experiment to detect a proton electric dipole moment, Rev. Sci. Instrum. **87**, 115116 (2016).
[39] S. Hacıömeroğlu and Y. K. Semertzidis, Hybrid ring design in the storage-ring proton electric dipole moment experiment, Phys. Rev. Accel. Beams **22**, 034001 (2019).
[40] C. Abel *et al.*, Measurement of the permanent electric dipole moment of the neutron, Phys. Rev. Lett. **124**, 081803 (2020).
[41] A. Andres, The first direct measurement of the deuteron electric dipole moment at the cooler synchrotron COSY, Dissertation, RWTH Aachen University, Aachen, 2024, 10.18154/RWTH-2024-12160.
[42] JEDI Collaboration, Replication data for: First experimental limit on the permanent electric dipole moment of the deuteron, Jülich DATA 10.26165/JUELICH-DATA/PCC4TE (2025).
[43] F. Abusaif, F. Hinder, A. Nass, J. Pretz, F. Rathmann, H. Soltner, D. Shergelashvili, R. Suvarna, and F. Trinkel, Compact beam position monitor using a segmented toroidal coil, Rev. Sci. Instrum. **96**, 033302 (2025).

End Matter

Models for polarization buildup—Two models have been developed for the single-bunch and pilot-bunch methods to describe the polarization buildup and to extract the resonance strength ϵ. Deviations from the ideal behavior described by Eq. (13) arise from decoherence and from deviations from the resonance frequency. Spin decoherence leads to a decay of the in-plane polarization, thereby reducing the effective contribution of spin rotation from horizontal to vertical polarization over time [25,32]. This effect must be taken into account, in particular for finite spin-coherence times, to reliably determine the resonance strength from the initial slope or the oscillation frequency. Deviations from exact resonance account for the finite precision of the phase-lock feedback [16].

Polarization buildup using a single bunch—Decoherence is taken into account by fitting the out-of-plane angle $\alpha(t)$ of the polarization vector and the total polarization $p_{\mathrm{tot}}(t)$ simultaneously, where

$$\alpha(t) = \arctan[p_v(t)/p_h(t)], \tag{B1}$$

$$p_{\mathrm{tot}}(t) = \sqrt{p_v(t)^2 + p_h(t)^2}, \tag{B2}$$

where $p_h(t)$ and $p_v(t)$ denote the in-plane and the vertical polarization, respectively. Note that the vertical polarization p_v corresponds to the spin component S_y in Eq. (13). Assuming an exponential decay of the in-plane polarization, characterized by

$$-\frac{1}{p_h(t)}\frac{\mathrm{d}p_h(t)}{\mathrm{d}t} = \text{const.} = B, \tag{B3}$$

this results in a nonlinear term for $\alpha(t)$, which includes the constant spin kick per turn $A = 2\pi\epsilon f_{\mathrm{rev}} \sin\varphi_{\mathrm{rel}}$ as one of its parameters [cf. Eq. (5.13) and (5.14) in [32]],

$$\tan[\alpha(t)] = \begin{cases} \tan(\alpha_0)e^{Bt}, & A = 0, \\ \frac{1}{2A}\left(\sqrt{E}\frac{D+\tan\left(\frac{t}{2}\sqrt{E}\right)}{1-D\tan\left(\frac{t}{2}\sqrt{E}\right)} - B\right), & E > 0, \\ \frac{1}{2A}\left(\sqrt{-E}\frac{D-\tanh\left(\frac{t}{2}\sqrt{-E}\right)}{1-D\tanh\left(\frac{t}{2}\sqrt{-E}\right)} - B\right), & E < 0, \end{cases}$$

$$\text{with} \quad D = \frac{2A\tan(\alpha_0) + B}{\sqrt{|E|}}, \qquad E = 4A^2 - B^2 \tag{B4}$$

and

$$\log\left(\frac{p_{\text{tot}}(t)}{p_{\text{tot},0}}\right) = \frac{1}{2}\log\left(\frac{2A + B\sin(2\alpha_0)}{2A + B\sin(2\alpha(t))}\right) + \begin{cases} \frac{B}{\sqrt{E}}\arctan\left(\frac{\sin(\alpha_0-\alpha(t))\sqrt{E}}{2A\cos(\alpha_0-\alpha(t))+B\sin(\alpha_0+\alpha(t))}\right), & E > 0, \\ \frac{B}{\sqrt{-E}}\operatorname{artanh}\left(\frac{\sin(\alpha_0-\alpha(t))\sqrt{-E}}{2A\cos(\alpha_0-\alpha(t))+B\sin(\alpha_0+\alpha(t))}\right), & E < 0. \end{cases} \tag{B5}$$

where α_0 and $p_{\text{tot},0}$ denote the initial out-of-plane angle and initial total polarization.

Polarization buildup using a pilot bunch—This case including decoherence and off-resonance behavior is discussed in [25]. The underlying formalism describes the time evolution of the polarization vector $\vec{p}$ after a time interval x, described in terms of a dimensionless variable,

$$x = 2\pi\epsilon_{\text{m}}(n - n_{\text{WF}}^{\text{on}}) \quad \text{or} \quad x = 2\pi\epsilon_{\text{m}} f_{\text{rev}}(t - t_{\text{WF}}^{\text{on}}), \tag{C1}$$

where n denotes the turn number and ϵ_{m} the measured resonance strength. Here, $x_{\text{WF}}^{\text{on}} = 2\pi\epsilon_{\text{m}} n_{\text{WF}}^{\text{on}}$ corresponds to the time when the rf Wien filter is switched on. The polarization vector is expressed as

$$\vec{p}(x) = \mathbf{E}(x) \cdot \vec{p}(x = x_{\text{WF}}^{\text{on}}), \tag{C2}$$

with $\vec{p} = (p_{\text{r}}, p_{\text{v}}, p_{\text{t}})^{\text{T}}$. The vertical component p_{v} is oriented along the invariant spin axis $\vec{n}$, the tangential component p_{t} is defined along the beam direction, and the radial component p_{r} lies perpendicular to both $\vec{n}$ and p_{t}. The polarization transfer matrix $\mathbf{E}(x)$ is given by Eq. (91) in [25]. The initial polarization condition for the experiment is defined by

$$\vec{p}(x = x_{\text{WF}}^{\text{on}}) = \begin{pmatrix} p_{\text{h},0}\sin(\varphi_{\text{rel},0}) \\ p_{\text{v},0} \\ p_{\text{h},0}\cos(\varphi_{\text{rel},0}) \end{pmatrix}, \tag{C3}$$

where $\varphi_{\text{rel},0}$ denotes the relative phase at the time the rf Wien filter is switched on. The initial in-plane polarization is given by $p_{\text{h},0}^2 = p_{\text{r},0}^2 + p_{\text{t},0}^2$, and $p_{\text{v},0}$ denotes the initial vertical polarization, which can be nonzero if the rotation of the vertical polarization into the horizontal plane by the rf solenoid is incomplete. While the vertical polarization remains preserved over time, an exponential decay of the in-plane polarization is assumed. The decoherence parameter Q, related to the spin-coherence time, τ_{SCT}, is defined as

$$Q = \frac{1}{2\pi\epsilon_{\text{m}} f_{\text{rev}} \tau_{\text{SCT}}}. \tag{C4}$$

The parameter δ characterizes the off-resonance behavior and is defined as

$$\delta = \frac{2\pi(f_s - f_{\text{WF}})}{f_{\text{rev}}}. \tag{C5}$$

In contrast to these corrections for the SCT, a detuned rf-Wien-filter frequency leads to a systematic shift of the measured resonance strength. The measured and the detuned resonance strength are connected via the dimensionless parameter ρ,

$$\sin(\rho) = \frac{\epsilon}{\epsilon_{\text{m}}} \text{ and } \cos(\rho) = \frac{2\delta}{4\pi\epsilon_{\text{m}}}, \tag{C6}$$

which allows for the determination of the unbiased resonance strength. The tangential, radial, and vertical components of the polarization are given by

$$\begin{aligned} p_{\text{t}} = &-e^{-Qx}\cos(\rho)\sin(x)\cos(\varphi_{\text{rel},0})p_{\text{h},0} \\ &+ e^{-Qx}\sin(\rho)\sin(x)p_{\text{v},0} \\ &+ e^{-Qx}\cos(x)\sin(\varphi_{\text{rel},0})p_{\text{h},0}, \end{aligned} \tag{C7}$$

$$\begin{aligned} p_{\text{r}} = &\left[e^{-2Qx}\sin(\rho)^2 + e^{-Qx}\cos(\rho)^2\cos(x)\right]\cos(\varphi_{\text{rel},0})p_{\text{h},0} \\ &+ (e^{-2Qx} - e^{-Qx}\cos(x))\cos(\rho)\sin(\rho)p_{\text{v},0} \\ &+ e^{-Qx}\cos(\rho)\sin(x)\sin(\varphi_{\text{rel},0})p_{\text{h},0}, \end{aligned} \tag{C8}$$

and

$$\begin{aligned} p_{\text{v}} = &-e^{-2Qx}\cos(\rho)\sin(\rho)\sin(\varphi_{\text{rel},0})p_{\text{h},0} \\ &+ e^{-Qx}\cos(\rho)\sin(\rho)\cos(x)\sin(\varphi_{\text{rel},0})p_{\text{h},0} \\ &+ \left[e^{-2Qx}\cos(\rho)^2 + e^{-Qx}\sin(\rho)^2\cos(x)\right]p_{\text{v},0} \\ &- e^{-Qx}\sin(\rho)\sin(x)\sin(\varphi_{\text{rel},0})p_{\text{h},0}. \end{aligned} \tag{C9}$$

Using the polarimeter, only the in-plane polarization,

$$p_{\text{h}} = \sqrt{p_{\text{r}}^2 + p_{\text{t}}^2}, \tag{C10}$$

and the vertical polarization can be measured. From the event rates in the polarimeter quadrants, the left-right

(ϵ_{LR}) and up-down asymmetries (ϵ_{UD}) are determined, which scale directly with the vertical and horizontal polarization, respectively,

$$p_{\mathrm{h}} \to \epsilon_{\mathrm{UD}}, \tag{C11}$$

$$p_{\mathrm{v}} \to \epsilon_{\mathrm{LR}}. \tag{C12}$$

Finally, both p_{v} and p_{h} are fitted simultaneously to the measured asymmetries and the resonance strength ϵ can be extracted for one map point.

Systematic uncertainties—Beam- and spin-tracking simulations accounting for misalignments of the ring magnets and beam-position monitors have been carried out. In addition, simulations employing uncertainties in the envisaged final rf Wien filter configuration were performed to assess their impact on the field orientation. Originally, an additional experimental run using this final rf Wien filter geometry, including the planned ferrite components, had been foreseen. This could not be realized, as COSY was shut down at the end of 2023, excluding also further dedicated measurements to experimentally constrain sources of systematic uncertainties.

Moreover, the Rogowski coils developed as beam-position monitors (BPM) at the entrance and exit of the rf Wien filter [43] had been commissioned during the beam time used for the measurements presented in this Letter. Consequently, local beam orbit monitoring within the rf Wien filter was limited, and beam-position information relied on BPMs located further upstream and downstream. As a result, possible deviations from the optimal beam orbit within the rf Wien filter could not be excluded. To address these limitations, additional simulations on the rf Wien filter fields were performed following the approach of Ref. [33]. In total 16 parameters were varied. These simulations included variations of both the rf Wien filter geometry and the beam parameters, including horizontal and vertical translations and rotations of the beam. The dominant contribution was found to originate from a rotation of the beam axis in the horizontal plane, as illustrated in Fig. 4. This could also explain the observed map-to-map variations, if one allows for map-dependent orbit changes in the rf Wien filter.

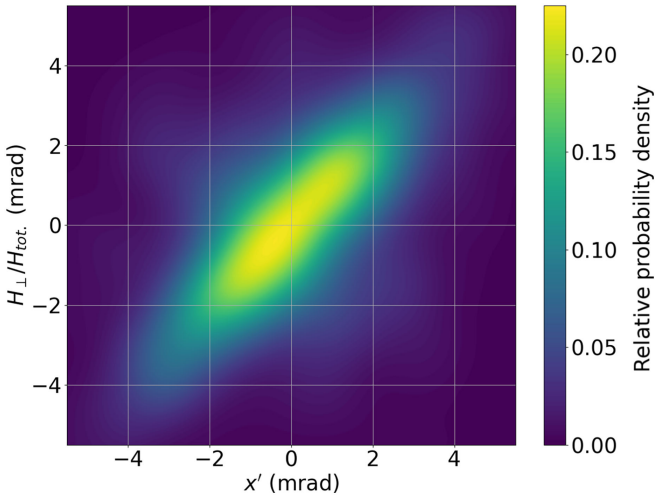

FIG. 4. Perpendicular contributions to the main (vertical) magnetic field as a function of a rotation of the beam axis in the horizontal plane (x'), illustrating the sensitivity of the field orientation to uncertainties in the beam parameters. The plot resembles a projection of the 16-parameter space onto the x' axis and is based on 800 full-wave simulations, further processed using a machine-learning-based sparse polynomial chaos expansion as discussed in Ref. [33]. Expected uncertainties in x' are in the order of 1–2 mrad. The colors indicate the probability for the $H_\perp$ contribution given at a certain x'.

Combining all identified sources of systematic uncertainty, the resulting uncertainty in the magnetic-field orientation and thus in the direction of the invariant spin axis can reach the level of a few milliradians, consistent with the observed systematic offset of the final result.